The 7th International Supercritical CO_2 Power Cycles Symposium
February 21 – 24, 2022, San Antonio, Texas
Paper # 164

Mechanical and Rotordynamic Test Results of a Supercritical CO_2 Compressor Operating Near the Critical Point

Jeffrey Moore, Ph.D.
Institute Engineer
Southwest Research Institute
San Antonio, TX

Stefan D. Cich
Group Leader
Southwest Research Institute
San Antonio, TX

Joshua Neveu, P.E.
Research Engineer
Southwest Research Institute
San Antonio, TX

John Klaerner
Engineer
Southwest Research Institute
San Antonio, TX

Jason Mortzheim
Senior Engineer, Mechanical
GE Global Research
Niskayuna, NY

Jeffrey Moore, Ph.D.

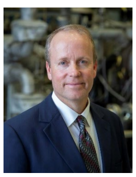

Dr. Jeffrey Moore is an Institute Engineer in the Machinery Section at Southwest Research Institute in San Antonio, TX. He holds a B.S., M.S., and Ph.D. in Mechanical Engineering from Texas A&M University. His professional experience over the last 30 years includes engineering and management responsibilities related to centrifugal compressors and gas turbines at Solar Turbines Inc. in San Diego, CA, Dresser-Rand (now Siemens Energy) in Olean, NY, and Southwest Research Institute in San Antonio, TX. His interests include advanced power cycles and compression methods, rotordynamics, seals and bearings, computational fluid dynamics, finite element analysis, machine design, controls, aerodynamics, and oxy-combustion. He has authored over 40 technical papers related to turbomachinery and has four patents issued. Dr. Moore has held positions as the Vanguard Chair of the Structures and Dynamics Committee and Chair of Oil and Gas Committee for IGTI Turbo Expo. He has also served as the Associate Editor for the Journal of Tribology and a member of the IGTI sCO_2 Committee, Turbomachinery Symposium Advisory Committee, the IFToMM International Rotordynamics Conference Committee, and the API 616 and 684 Task Forces.

Stefan Cich

Stefan Cich is a Group Leader in the Machinery Section at Southwest Research Institute (SwRI) in San Antonio, TX. He holds a B.S. in Aerospace Engineering from the University of Texas at Austin. His professional experience over the last 9 years has been focused around the design, analysis, and development of high pressure equipment and turbomachinery. His first job for two years focused on high pressure hydraulic fracturing equipment. While at SwRI, his main focus has been on various advanced turbines and compressors for a variety of applications. Much of it has been on the development and testing of equipment for use in super critical CO_2 power cycles. This includes multiple 16 MW turbines, 2.5 MW compressors, 5.5 MW to 55 MW recuperators, and a 2 MW heater along with all the necessary equipment to fully operate a power loop. Through all of this, he has gained experience in various ASME and API codes, design and manufacturing of advanced equipment through advanced *manufacturing processes, complex stress and thermal analysis of high temperature and high pressure equipment, and testing and operating procedures of new age power cycles.*

Joshua Neveu

Josh Neveu is a Research Engineer in the Machinery Section at Southwest Research Institute in San Antonio, TX. He holds a B.S. in Mechanical Engineering from Texas A&M University and is a Licensed Professional Engineer in the State of Texas. His professional experience over the last 6 years has been focused around the design, management, and commissioning of industrial refrigeration and power generation systems. While at SwRI, his main focus has been on the development, testing, and control of equipment for use in supercritical CO2 power cycles. This includes turbines, compressors, and heat exchangers, along with the necessary control systems to fully operate a power loop. Through all of this, he has gained experience in various testing and operating procedures of new age thermodynamic cycles.

John Klaerner

John Klaerner is an Engineer in the Rotating Machinery Dynamics Section at Southwest Research Institute® in San Antonio, Texas. He holds a B.S. in Mechanical Engineering from Texas A&M University where he began his studies of large machinery and various power systems. His professional experience at SwRI has allowed for continuing in machinery design and thermal analysis, mostly related to equipment being used in Supercritical Carbon Dioxide (sCO_2) cycles. These focuses have led to further experience in instrumentation, commissioning, and testing of individual cycle components, full sCO_2 test loops, and other energy storage programs.

Jason Mortzheim

Mr. Jason Mortzheim is a senior mechanical engineer at the GE Global Research Center in Niskayuna, NY. He has a B.S. in aeronautical engineering from Rensselaer Polytechnic Institute and a M.S. in aerospace engineering from Georgia Institute of Technology. His area of research has been centered on improving fossil power combined cycle plant efficiency including both steam and gas turbines. Mr. Mortzheim initial area of research focused around advanced seal designs where he has held various roles spanning his 19 year professional career. He has utilized computational methods, both commercial CFD and in-house flow solvers, advanced experimental campaigns including industry leading test rig designs, complete to post commercial operation validation to develop state of the art seal technology ranging from brush seals to film riding seals. Mr. Mortzheim is currently the Principal Investigator for DoE contract, EE0007109 related to advanced sCO_2 power cycle compression technology and the GE Principal Investigator supporting DoE contract, FE0028979, 10 MWe sCO_2 Pilot Plant Test Facility.

ABSTRACT

Supercritical Carbon Dioxide (sCO_2) power cycles can provide higher thermal efficiency compared to traditional steam-based cycles for both fossil and alternative energy sources. The small turbomachinery of these cycles reduces capital costs due to smaller equipment footprints and permit rapid transients to follow demand swings of the electric power grid with high variable renewable energy (VRE) penetration. Testing has been completed on a 2.5 MW Supercritical Carbon Dioxide (sCO_2) compressor operating near the critical point of pure CO_2, which is sized to provide compression on a 10 MWe power plant. Traditionally, operation of a centrifugal

compressor near the critical point has been avoided due to the rapidly changing fluid properties and the potential to enter the liquid-vapor dome. The advantage of such operation is lower head requirement which needs much less compression power leading to an overall increase in thermal efficiency of this various power cycles. The compressor developed specifically for this application pushes many current technology limits, including but not limited to: bearing and seal technologies, rotordynamics, compact machinery packaging, variable geometry, and high-density, high-speed compression. The high density results in impressive pressure rise, increasing the pressure from 86 to 266 bar in a single stage. The forces acting on the compressor and diaphragm must be carefully managed as well as the thrust load. Due to these large changes in density with temperature, range extension is required to accommodate the resulting swings in volume flow in order to maintain high compression efficiency over a range of ambient temperatures. High flow range was accomplished using variable inlet guides vanes (IGVs). This application represents the highest density centrifugal compressor reported in the literature with densities up to 71% of water. This paper will present the measured vibration and seal data and describe remedies to a vibration issue encountered. A dry gas seal failure was encountered and discussed along with a cold start-up with operation within the liquid-vapor dome.

INTRODUCTION

sCO_2 power cycles have received significant interest and development through both commercial and government sponsored efforts due to the potentially greater thermodynamic efficiency, small equipment size, and relative safety of CO_2 as the working fluid. The cycle reduces capital cost due to smaller footprint of the equipment. Lower thermal mass permits faster thermal cycles allowing the power plant to follow the highly cyclic demand of the future electrical grid due to variable renewable energy. While compressing CO_2 is not novel, doing so at a suction condition near the critical point of the gas (73.8 bar, 31ºC) is traditionally avoided. However, the benefit of supercritical compression is higher density and lower head required, resulting in lower compression power in the cycle. The other advantage of the high density is that fewer stages are required. In fact, the current compressor was designed for a pressure rise from 85.5 to 265.6 bar and was accomplished in a single impeller stage requiring about 1.8 MW with an impeller only 149 mm (5.86") in diameter while rotating at 27,000 rpm. This high power density, large stage rise, and small size results in a challenging mechanical, aerodynamic, and rotordynamic design and will be discussed in this paper along with test results. In addition, operation near the dome results in large changes is gas properties with relatively small changes in inlet temperature. For example, near the dome, CO_2 changes density by a factor of 2 with only a 10°C change in temperature. Since the cycle requires a given mass flow, and centrifugal compressors are volume flow dependent, design features were added to accommodate a wider range of operating flow, namely moveable IGVs. While variable IGVs are not unique, their application to a high pressure compressor with such a large stage rise is certainly novel. Pressure and temperature in the test loop can change quickly, requiring coordination between coolers and the amount of mass in the loop.

The U.S. DOE SunShot project focused on the development of a high temperature 10 MWe sCO_2 turbine (Moore, et al. 2015, 2018, 2020) and tested in a 1 MWe test loop. Other researchers have also developed the sCO_2 power cycle and equipment (Hexemer, 2014, Spadacini, et al., 2018). McClung et al. (2018) is developing a 10 MWe SCO_2 test facility named the STEP project funded by the U.S. DOE. Figure 1 shows the overall cycle model and design conditions that are used to develop the turbomachinery for the cycle. The Apollo program described in this paper focuses on the design and testing of the main compressor for this recompression Brayton cycle. More information related to the development and initial testing of the Apollo compressor is described by Cich and Moore et al. (2018, 2020 and 2021). This paper explores the unusual vibration behavior encountered during testing and how it was remedied. A dry gas seal failure also occurred and is discussed. Finally, the cold start-up from inside the liquid-vapor dome was performed and data provided.

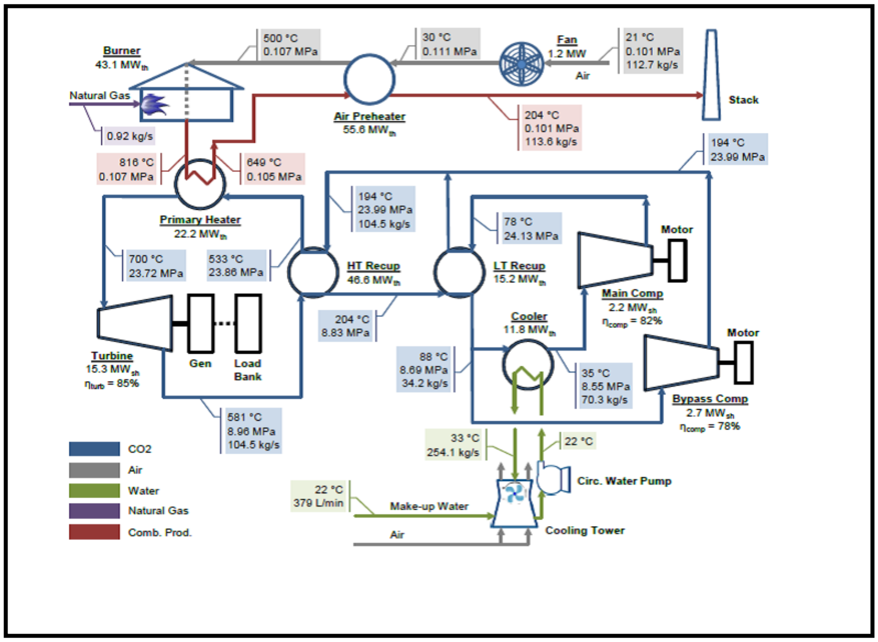

Figure 1 - Proposed Recompression Brayton Cycle with sCO_2

Compressor Design

The final compressor layout is shown in Figure 2. The compressor was designed as a back-to-back concept accommodating both the main and bypass compressor in the sCO_2 recompression Brayton cycle. However, for the initial development testing, only the main compressor impeller was implemented, and the two recompressor impellers are represented as simple disks to capture the rotordynamic influences. A modular bundle in a barrel style casing is utilized so that it can be installed and removed from the case as an assembly greatly simplifying installation and maintenance. The bundle utilizes non-split diaphragms made possible with the modular rotor construction with a central tie-bolt. The main compressor diaphragm must support 170 bar pressure differential and contains the variable IGV mechanisms. Due to the relatively small diameter of the main impeller, the hub diameter at the impeller is smaller than the dry gas seal diameter, which is driven by the journal bearing, coupling, and inboard thrust bearing arrangement, making a traditional shrunk-on impeller impossible without unacceptably poor rotordynamic behavior. The modular design solves this design challenge while maximizing rotor diameter along the shaft. In order to improve the structural integrity of this high power density impeller, 5-axis electrode discharge machining (EDM) was utilized in its manufacturing, followed by extrude-honing to improve surface finish resulting in a single-piece part (no welding or brazing) and was overspeed tested to 120% of running speed. Careful sizing of the balance piston seal minimizes the axial load on the thrust bearing.

The head on both ends accommodate dry gas seals to minimize shaft end leakage. Large studs and nuts retain the endcap, which also supports the thrust and journal bearing housing on the left. On the right, the other head supports the radial bearing housing and coupling guard adapter. The casing is rated to 338 bar (4,900 psi) and utilizes Grayloc™ style nozzle connections.

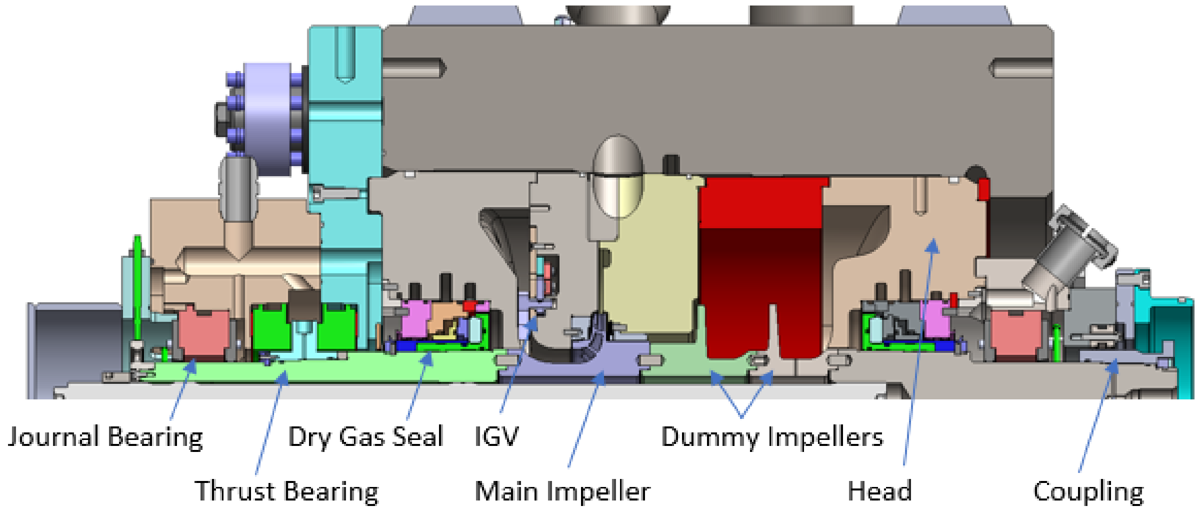

Figure 2 - Final Apollo Compressor Layout

ROTORDYNAMIC ANALYSIS

A full API 617 Level 2 rotordynamic analysis was performed. Given the high density and pressure rise, close attention was paid to the contribution of seal forces and deformation under pressure. Figure 3 shows the rotordynamic experience chart of a major compressor vendor along with the API Level 1-2 line and the Apollo application. This figure plots the critical speed ratio vs. the average gas density in the compressor. The SunShot turbine is shown for reference. The Apollo compressor is clearly well outside the industry experience due to the high density. Therefore, a full level 2 stability analysis is performed including the labyrinth and hole pattern damper seal as well as the impeller coefficients. Swirl brakes are integrated into the impeller eye and balance piston seal.

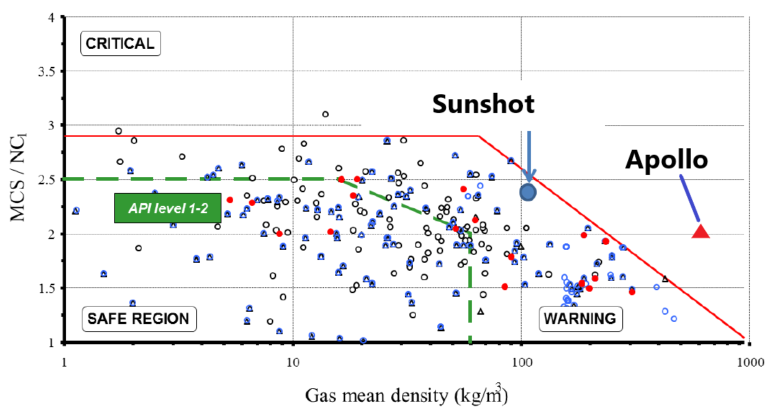

Figure 3. Rotordynamic Experience Chart from Moore (2006) with SunShot Turbine and Apollo Compressor Rotor Added

The rotor model is shown in Figure 4, using 1-dimensional beam elements. The multi-layer analysis consists of each stub shaft, impeller, spacers, and the tie bolt. The impellers, dummy wheels, thrust collar, and coupling are modeled as added masses. The oil film stiffness and damping is in series with the squeeze film damper stiffness and damping. The tilting pad bearings are manufactured using wire EDM and contain an integral squeeze film damper.

Comparison of the rotordynamic behavior with and without the squeeze film damper will be made later in the paper. Figure 5 shows the imbalance response using four times the API unbalance (4 x 4W/N) showing a well damped first critical speed and good separation to the bending critical speed, which is well above running speed.

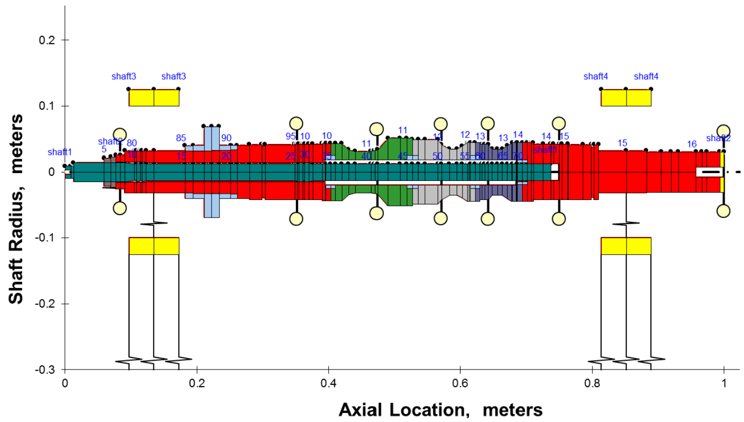

Figure 4 - Rotordynamics Shaft Model

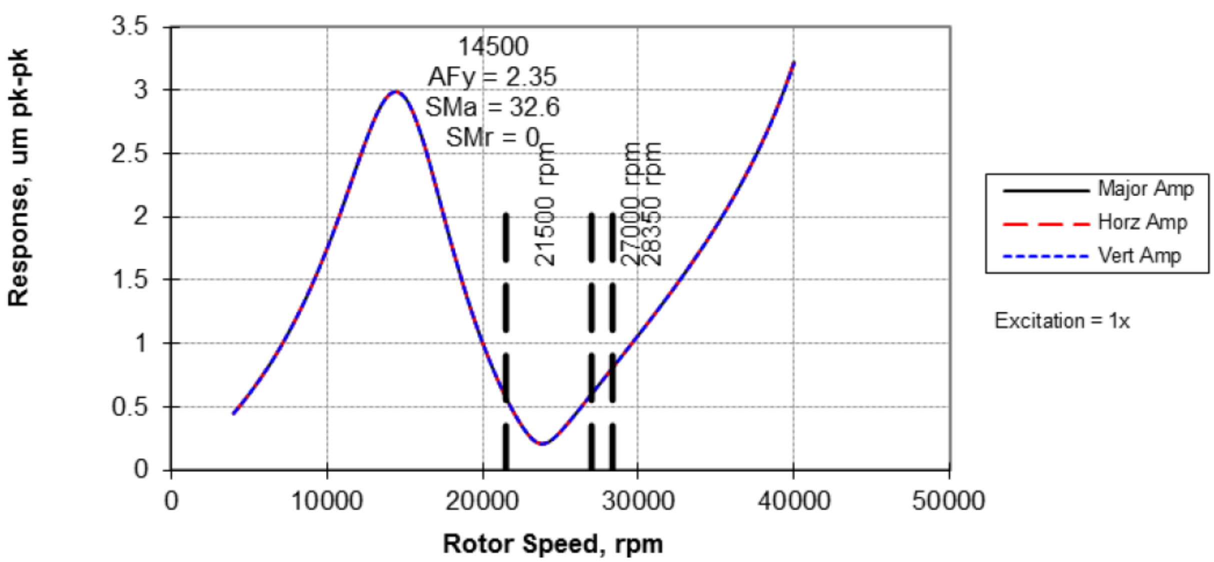

Figure 5 - Bearing Vibration Response with Mid-Span Imbalance

As previously mentioned, a Level 2 rotordynamic stability analysis requires that all seals and impeller force coefficients be included in the model. Figure 6 shows the results of that analysis with bearings only (blue) and with seal effects included (green) by plotting the calculated logarithmic decrement (log dec) for the first forward whirling model versus applied aerodynamic cross-coupling placed at the impeller location.

The aerodynamic excitation is determined using two methods: API modified Wachel (per API 617, 7th Ed.); and the Moore-Ransom method derived from CFD. The API modified Wachel method is calculated per Eq. 1 :

$$K_{xy} = \left(\frac{189{,}000}{N}\right)\sum\left(\frac{Hp}{D \cdot B_3}\right)\left(\frac{\rho_d}{\rho_s}\right)\left(\eta^2\right) \tag{1}$$

where Hp is the stage power (Hp), N is the rotor speed (rpm), D is the impeller diameter (in), B_3 is the diffuser passage width (in), ρ_d is the stage discharge density, ρ_s is the stage suction density. Moore et al. (2007) presented the following formula as an alternative formulation to the Wachel Eq. 2 based on a parametric study varying several operating parameters independently.

$$K_{xy} = \frac{C_{mr}\ \rho_{dis}\ U^2\ L_{shr}}{Q/Q_{design}} \tag{2}$$

where, K_{xy} = cross-coupled stiffness of impeller (lb/in) [N/m]
C_{mr} = 0.0016 (US Customary units)
= 7.3 [SI units]
= impeller cross-coupling coefficient
ρ_{dis} = discharge density (lbm/ft^3) [kg/m^3]
U = impeller outer radius tip speed (ft/s) [m/s]
L_{shr} = axial length of shroud from impeller eye seal to impeller tip (in) [m]
Q/Q_{design} = flow relative to design flow

For this application, the API method calculates a cross-coupling of 4.8E6 N/m (27,400 lb/in), while the Moore-Ransom method predicts a value of 4.6E6 N/m (26,000 lb/in) if no impeller eye swirl brake is incorporated and only 7.5E5 N/m (4300 lb/in) with a swirl brake. Even though a swirl brake was used, the API value is used in order to be conservative. Figure 6 shows a log dec of 0.78 with 100% of the API impeller excitation and a stability margin of 6, which is considered quite stable.

Finally, Figure 7 shows the sensitivity of clearance taper of the balance piston seal on the rotordynamic stability. Due to the high pressure and density, the hole pattern seal has a large influence and can drive the compressor unstable if any divergence of the seal clearance is encountered. The seal installation is designed to have low pressure behind the seal that helps to minimize elastic deformation of the seal. Furthermore, a positive taper is machined into the seal (inlet radial clearance is a few mils larger that the exit of the seal) to provide further margin against instability.

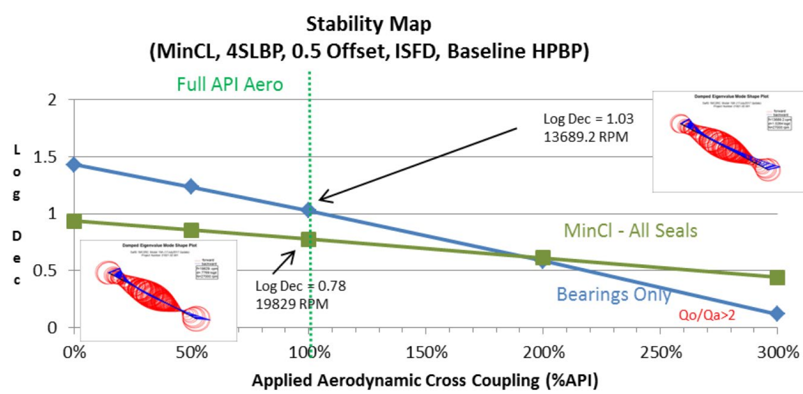

Figure 6 - Rotordynamic Stability Map (Minimum Bearing Clearance Bearings)

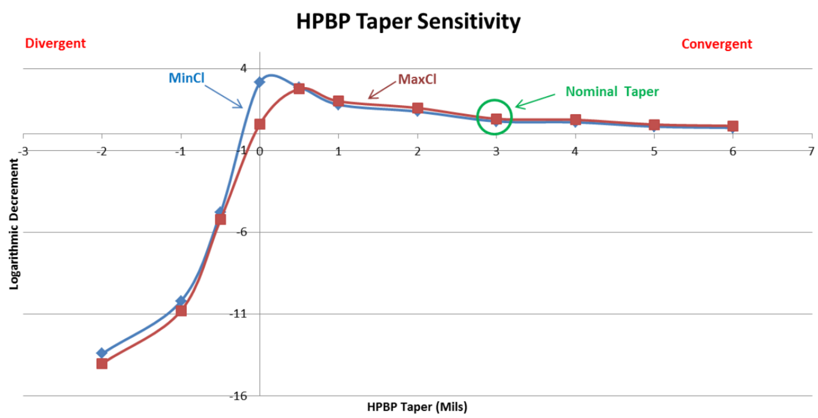

Figure 7 - Hole Pattern Balance Piston Seal Taper Sensitivity

TEST LOOP DESIGN

The compressor flow loop at SwRI was utilized for this test program with a few modifications. The loop contains 600# ANSI flanges nominally rated to 94 bar (1,360 psi). A high pressure discharge throttle valve was added just downstream of the compressor with a V-cone style flow meter following the valve. The flow meter was placed on the warm section of the loop to improve the gas property accuracy of the flow rate calculation. Other modifications include the addition of the chiller heat exchanger, which is the same one used in the SunShot test program. This chiller was placed in a parallel branch to the main piping, since all of the flow could not be sent through the relatively small heat exchanger. But the arrangement allowed the lower temperature condition conditions to be achieved. A second gearbox was added to the 3 MW test skid, increasing the speed capability from 14,000 rpm to 28,350 rpm. A second lube oil skid was added to accommodate the compressor. The dry gas seal panel designed for the SunShot turbine was employed on the Apollo test program.

Existing infrastructure that was repurposed is shown in Figure 8.

Figure 8 - Existing Piping for Compressor Test Loop at SwRI

Figure 9 shows the process and instrumentation diagram (P&ID) showing how the Apollo compressor ties into the existing test loop. The design permits the testing of the main and recompressor providing independent flow, temperature, and pressure measurement in accordance to ASME PTC-10 guidelines; however, for this test program only the main compressor is tested.

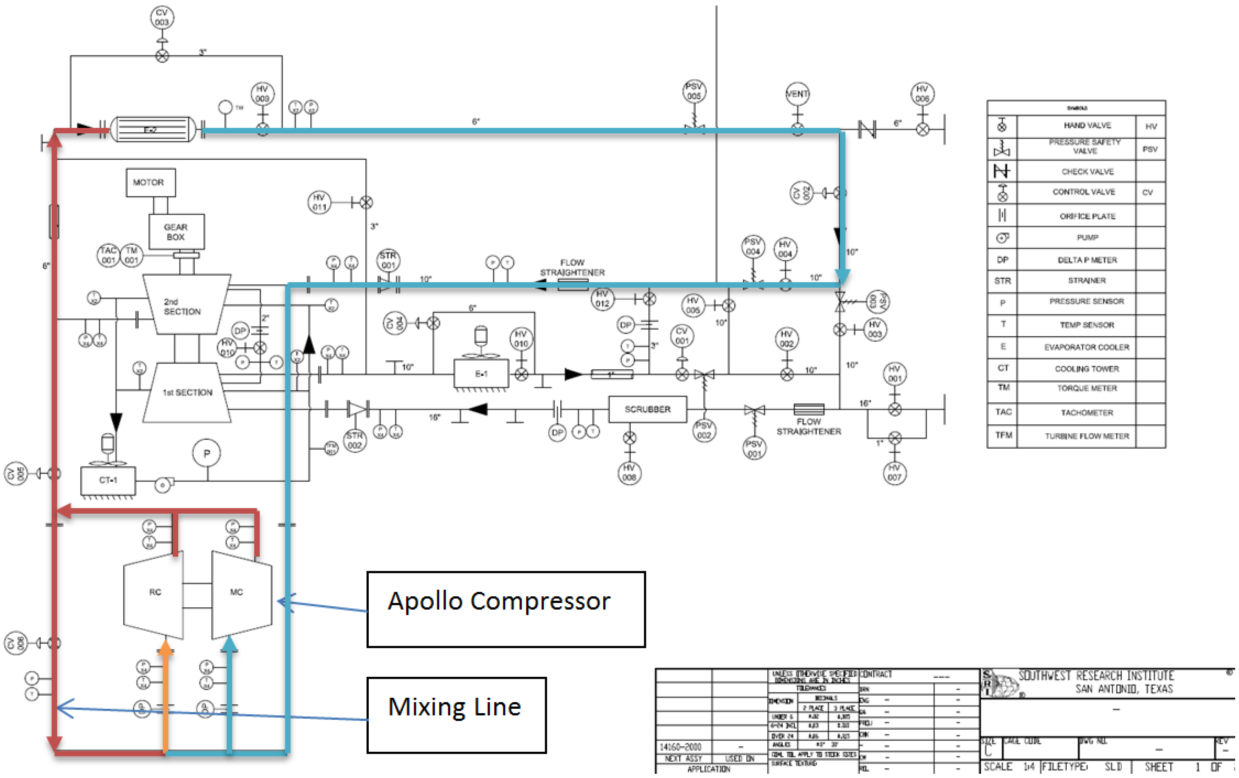

Figure 9 - Process and Instrumentation Diagram

COMPRESSOR MANUFACTURING AND ASSEMBLY

The built-up rotor was manufactured with precision fits, assembled, and final ground for the critical surfaces resulting in low shaft runout as shown in Figure 10. The thrust disk is hydraulically installed and final low-speed balance performed. Modal tests were performed to verify the free-free natural frequencies of the rotor reasonably matched the rotor model. The casing components were assembled without the rotor and custom plugs were made in place of the dry gas seals to perform a hydro test per API 617 requirements. Figure 11 shows the assembled compressor on the test stand with all piping and instrumentation installed.

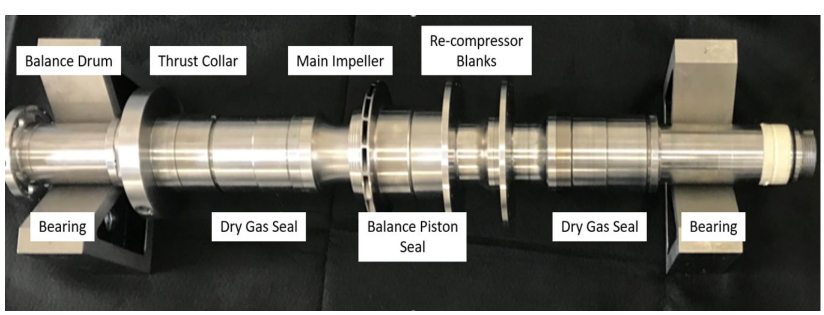

Figure 10 - Rotor Assembly

Figure 11 - Assembled Compressor on Test Stand

TEST RESULTS

Once all critical functional tests were performed including leak test, data acquisition, control, valve action, and variable frequency control (VFD) function, compressor break-in and mechanical testing of the compressor began. All mechanical parameters including bearing temperatures, dry gas seal parameters, and vibrations were well within limits. Overall vibrations were less than 22 um p-p (0.87 mils p-p) with essentially no subsynchronous vibration and bearings temperatures less than 96°C (205F°). Next aerodynamic testing at low pressure was performed at three IGV setting angles at the design speed of 27,000 rpm. Cich and Moore et al. (2020) provides an overview of the mechanical test data, and Cich and Moore et al. (2021) shows the low and high pressure performance data, which is provided in Figure 12. The results show the effectiveness of the variable IGVs to reduce the flow capacity of the compressor. In addition, comparing the choke line between the low and high pressure conditions shows the effect of Mach number due to the decreasing speed of sound of the supercritical fluid, especially when operating near the dome (e.g. 95°F data).

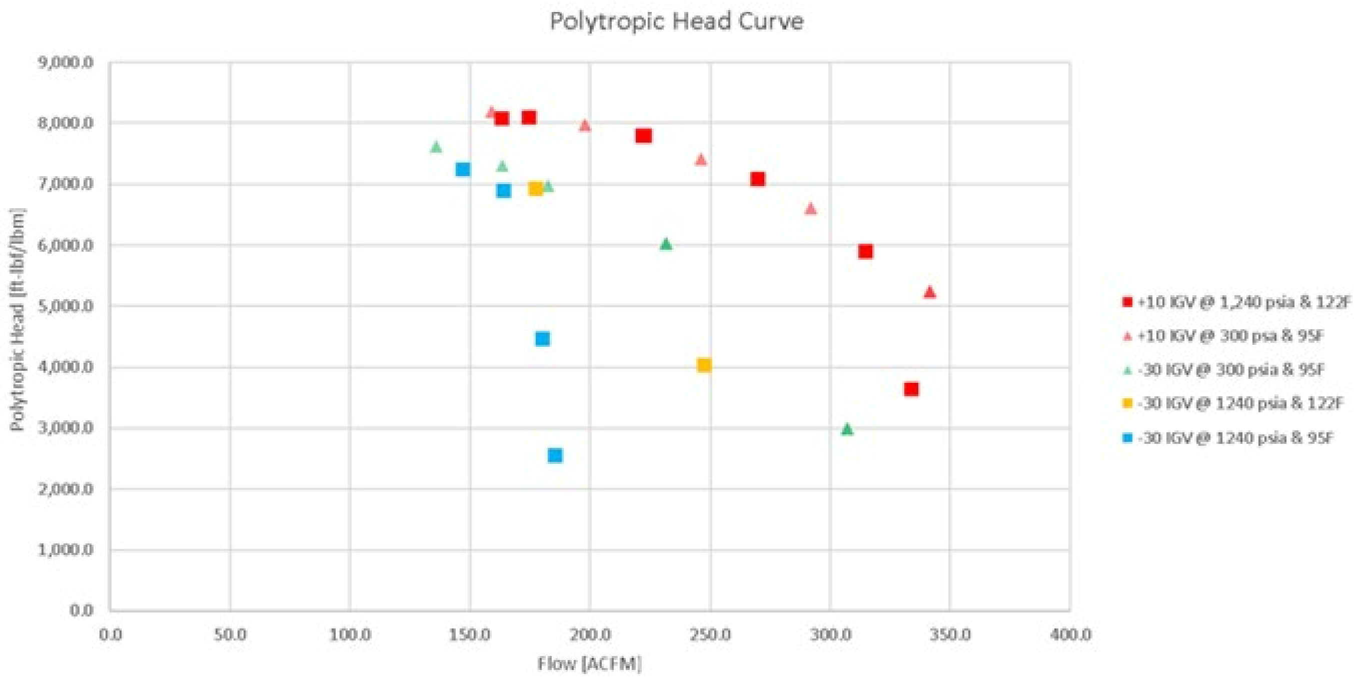

Figure 12 - Measured Compressor Maps at Low and High Pressure Suction Conditions

VIBRATION CHALLENGES

Initial sCO_2 compressor testing showed high sub-synchronous vibrations (Figure 13), and full speed was not reached. The spectrum showed a relatively low response, which was broadband and unsteady in nature and centered around a frequency of 30-40 Hz, with higher amplitude on the drive end. Note that peak-hold averaging was used to measure the maximum amplitude at each frequency. This frequency is well below the first natural frequency and did not possess the characteristic of a distinct frequency of either rotordynamic instability or a rotating stall. The excitation has the characteristics of an unsteady forced vibration.

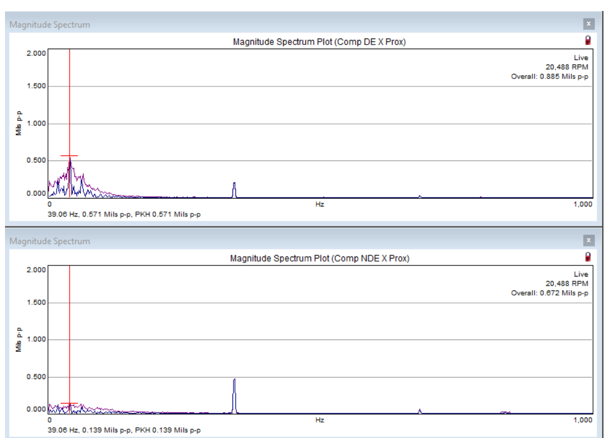

Figure 13 – Bearing Vibrations during Initial Testing at sCO_2 Conditions before Discovery of Balance Piston Seal Error

In order to determine the effect of density on the vibration response, the compressor was slowed to 14,150 rpm, and spectra were captured while reducing suction pressures from 85.2 barg (1,236 psia) down to 70.1 barg (1,016 psi) and densities as shown in Figure 14. The peak subsynchronous vibration is roughly proportional to the inlet density. This result reinforces the theory that the vibration is caused by a disturbance in the flow, and its magnitude is proportional to density.

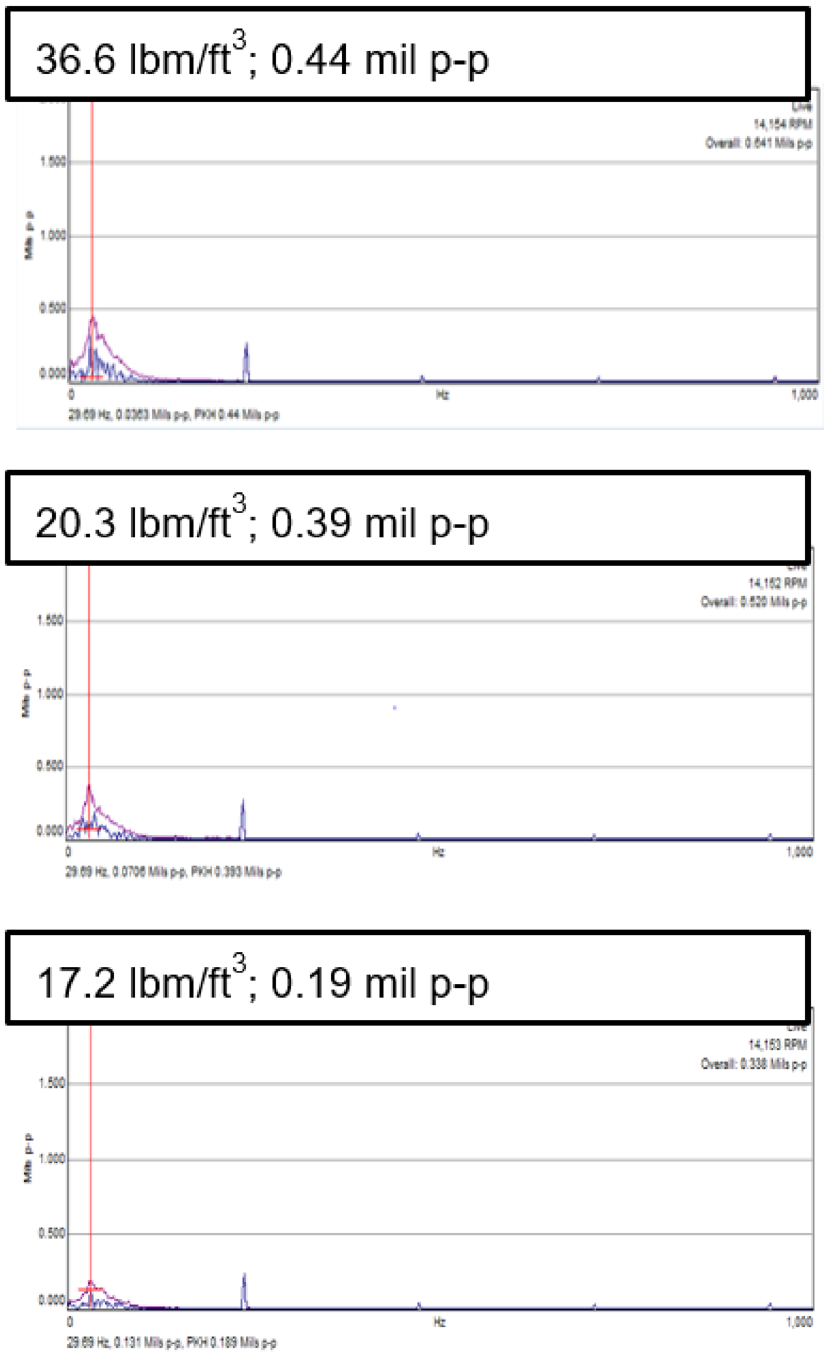

Figure 14 - Effect of Density on Subsynchronous Vibration

Following disassembly, it was discovered that the balance piston was not made with a positive taper as described above. According to Figure 7, the effective damping of the seal with no taper is near zero. While it was believed that the forcing function was not coming from the seal, increasing the damping at the seal would improve the response. Therefore, a new seal was made with the correct amount of positive taper, and the compressor was reassembled. The seal was returned using bolts instead of a spiral-lock style ring as shown in Figure 15.

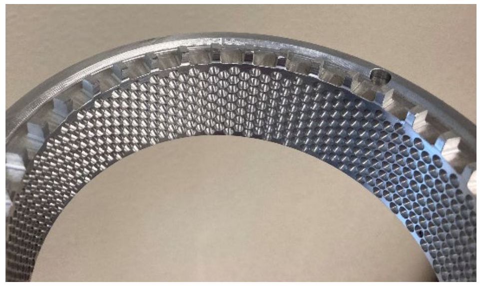

Figure 15 - Impeller Balance Piston Seal with Design Changes

After the balance piston seal was replaced, the compressor was re-tested again with a +10° IGV setting at low pressure confirm performance followed by full pressure tests. The vibration response was better and allowed full speed operation (27,000 rpm) at 36.4˚C (97.5˚F) inlet temperature and 1,200 psia inlet pressure as shown in Figure 16. The vibrations were near limits, so an attempt to reduce density and approach hot day conditions was made. A dry gas seal failure occurred at around 41.6°C (107°F) inlet temperature. The temperature was changing slowly and is unlikely the cause of the seal failure.

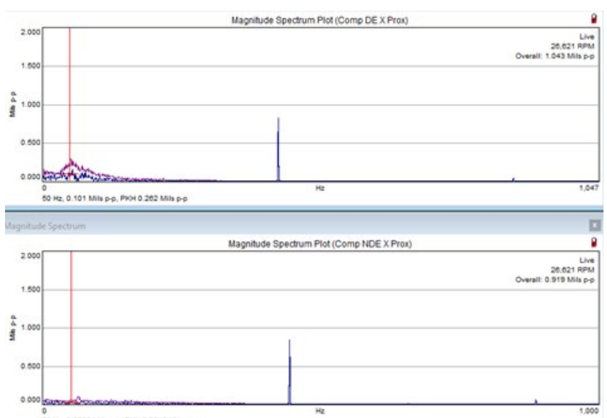

Figure 16 - Vibration Spectrum Following Balance Piston Modifications

Figures 16 and 17 show the vibration waterfall plot and waveform at the moment the failure occurred which showed both high vibration and radial shift in the position of the shaft. Figure 19 shows a photo of the failed seal after removal. The compressor shut down immediately due to high seal vent leakage (blew instrumented rupture disk). This high vent leakage went away after the compressor shut down due to the carbon dust from the seal ring plugging up the leakage annulus inside the seal. Initially the team thought the seal reseated itself, but when an attempt to rotate the shaft by hand was impossible, the decision was made to disassemble the compressor. Figure 19 shows the damaged seal.

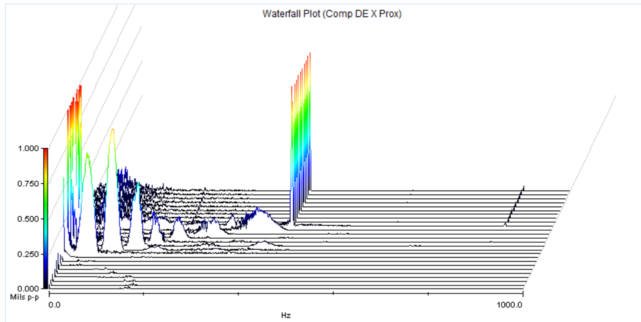

Figure 17 - Waterfall Plot During Dry Gas Seal Failure

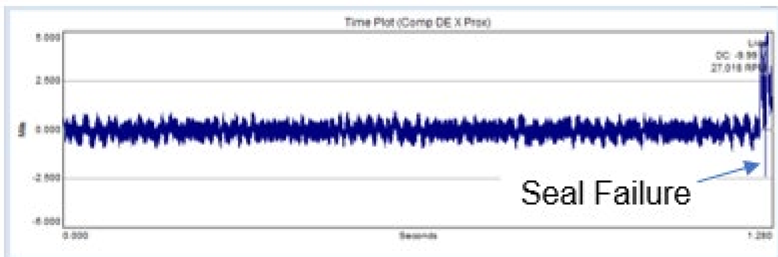

Figure 18 - Vibration Waveform During Dry Gas Seal Failure

Figure 19 - Photo of the Failed Dry Gas Seal

A root cause failure investigation was initiated in partnership with the seal manufacturer. It was determined that a bad lot of seal material was obtained from their supplier for the silicon carbide seal ring. The team had already started working with a second seal supplier, so the decision was made to switch to that seal, which was a direct retrofit of the original.

BROADBAND SUBSYNCHRONOUS VIBRATION

In order to better understand the source of the subsynchronous vibration, a CFD analysis was performed of the inlet with the +10° IGV setting and the exact operating conditions during the first test. Due to the compact size of the compressor and the high pressure nozzle case penetration, a relatively small inlet plenum was incorporated resulting in less than ideal flow behavior around the IGVs. Figure 20 shows the computed flow field with separation around some of the vanes for this setting angle. This flow disturbance makes its way downstream as indicated by the nearly 2:1 variation in axial flow velocity entering the impeller. While this result is from a steady-state CFD analysis, separation is generally unsteady with large eddies shedding off of the blades. Sezal et al. (2016) performed a CFD and test campaign and showed similar levels of flow variation including separation on some of the vanes. Due to the high pressure case design, the inlet nozzle could not be expanded to smooth the transition into the plenum and is partly responsible for the high axial velocity variation. These phenomena could explain the flow frequency, broad-band vibration observed in the test. Since the lift of an airfoil is a linear function of density, this theory can explain why the excitation force magnitude was proportional to density in the tests.

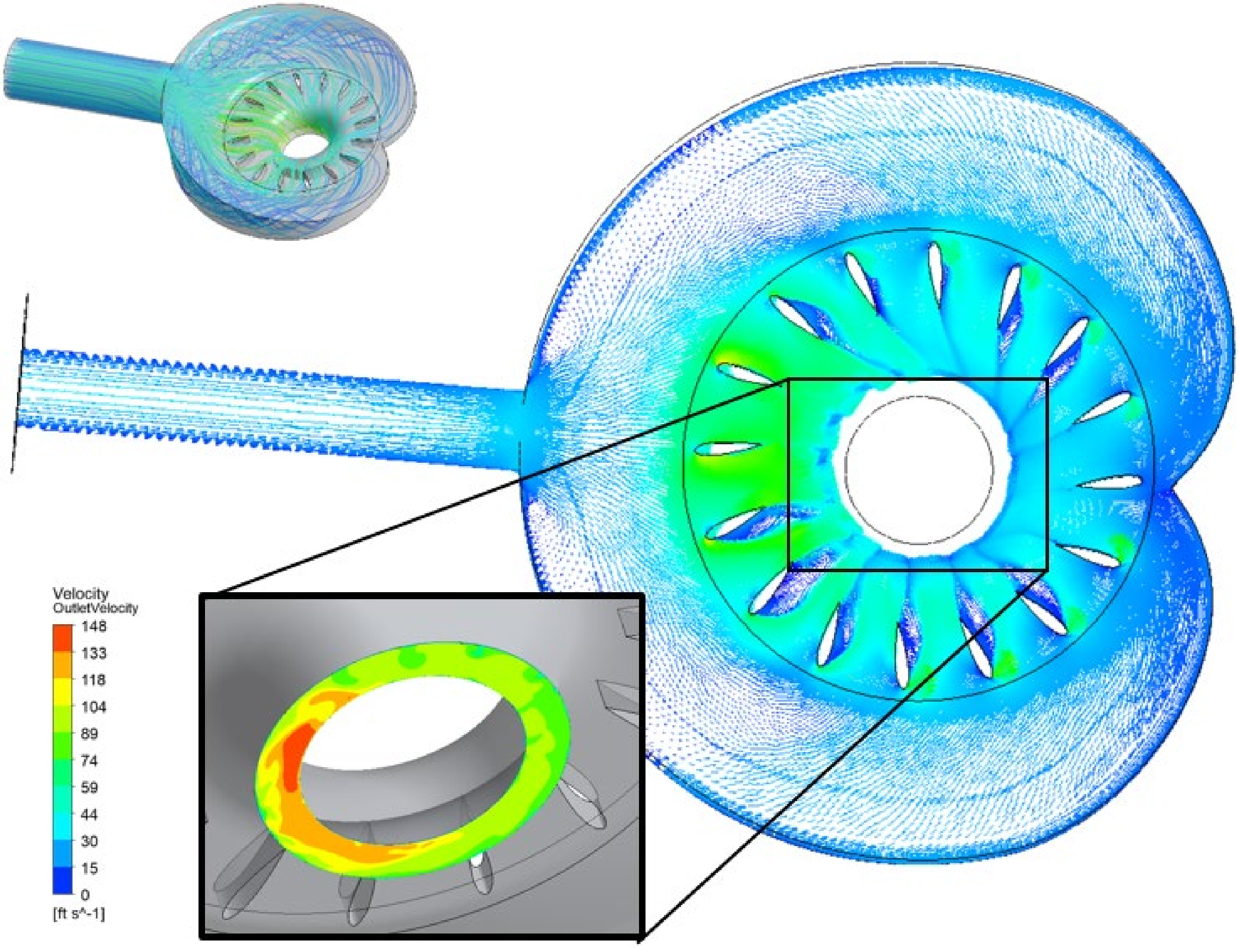

Figure 20 - Inlet Plenum CFD Analysis, +10° IGV Setting

Since redesigning the inlet was not feasible given the space constraints, the bearings were modified to improve their dynamic response at these low frequencies. One drawback of placing a squeeze film damper (SFD) in series with a journal bearing is reduced dynamic stiffness at low frequency. This fact is shown in Figure 21, where the dynamic stiffness for the tilt-pad bearing pads (blue), the squeeze film damper (red), and the total dynamic stiffness (green) are shown. Notice that the equation for dynamic stiffness includes the damping term. By eliminating the squeeze film damper, the dynamic stiffness at 2,000 rpm (33 Hz) can be increased by a factor of 7 (going from green to blue curve). Figures 22 and 23 show the unbalance response and stability map for the locked SFD case. Comparing these results to Figures 5 and 6 show slightly higher amplification factor for the first critical speed but nearly identical log dec (0.78 vs 0.76).

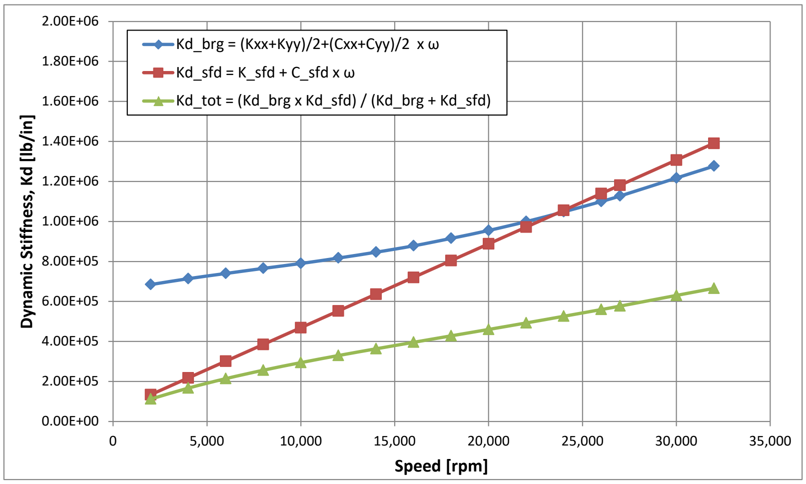

Figure 21 - Dynamic Stiffness Prediction with and without Squeeze Film Damper

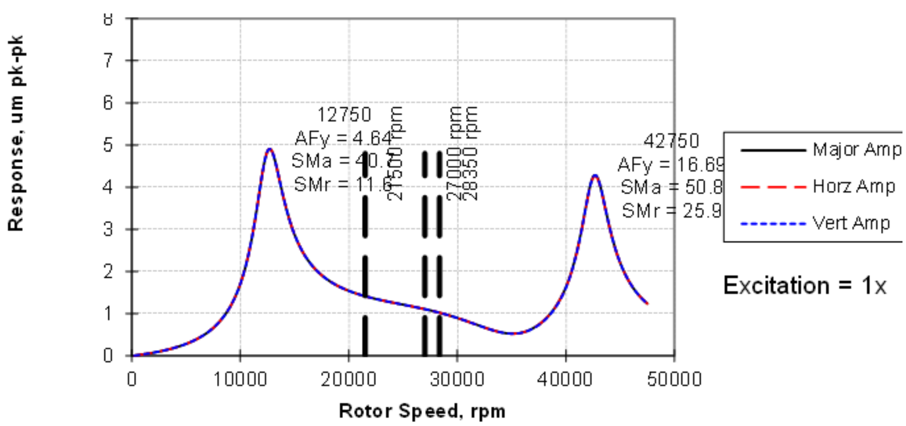

Figure 22 - Unbalance Response with Locked SFD

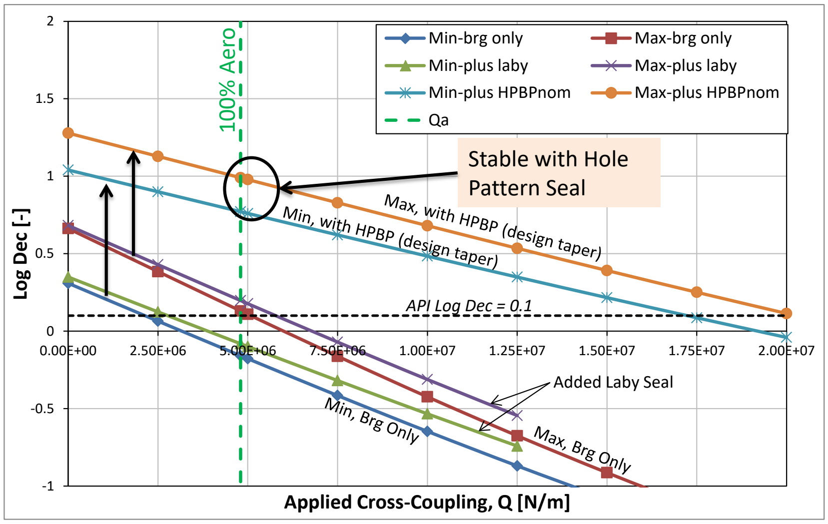

Figure 23 - Stability Map with Locked SFD

The bearings were modified by installing dowel pins to lock up the squeeze film dampers as indicated in Figure 24. While the rotordynamic system would lose some damping, the hole pattern damper seal provides more than adequate damping to maintain a stable rotor. Figures 25 and 26 compare the vibration with and without SFD with at nearly identical operating conditions with +10° IGV setting. While the subsynchronous vibration still exists, its magnitude has been reduced by a factor of four, and the overall vibration has dropped considerably, allowing for full speed and pressure operation well below vibration limits.

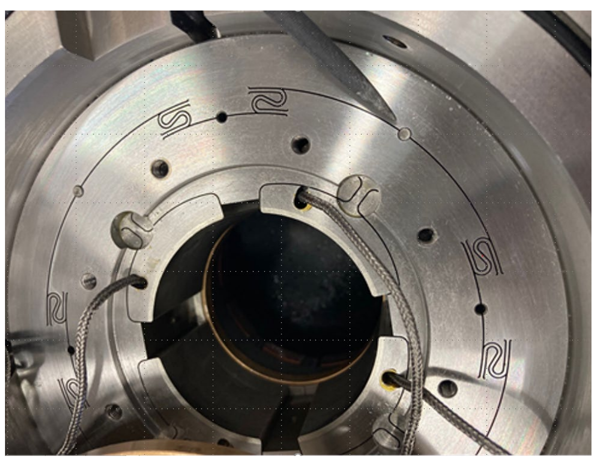

Figure 24 - Photo of SFD with Dowel Pins Installed

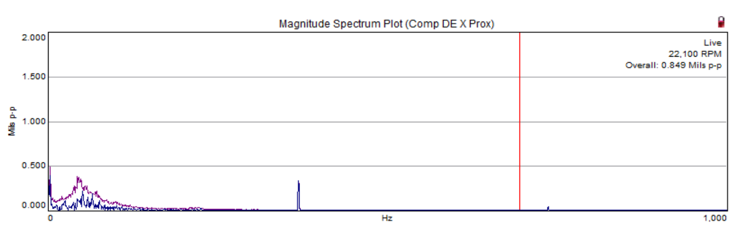

Figure 25 -Vibration Spectrum with SFD, Ps=1220psi, Ts=97F, N=22,100 rpm, 70% throttle, +10 IGV

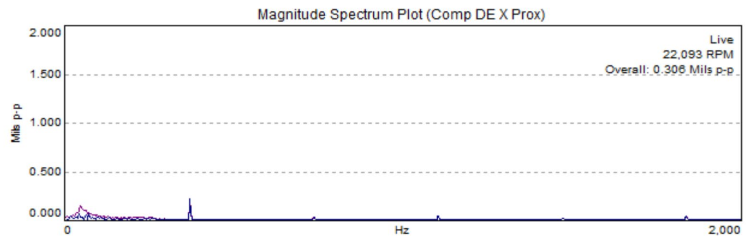

Figure 26 - Vibration Spectrum without SFD, Ps=1214psi, Ts=103F, N=22,093 rpm, 68% throttle, +10 IGV

FINAL TEST

The final test was made with -30 Deg IGV while operating at these conditions:

P1=1,248 psi, P2=,3341 psi, 27,000 rpm

At these conditions, the discharge density is 710 kg/m3 (44.5 lbm/ft^3), which is 71% of water. This discharge density is the highest reported in the literature for a high-speed centrifugal compressor. The vibration spectrum at this condition is shown in Figure 27 and shows very low subsynchronous vibration at this IGV setting and no signs of rotordynamic instability.

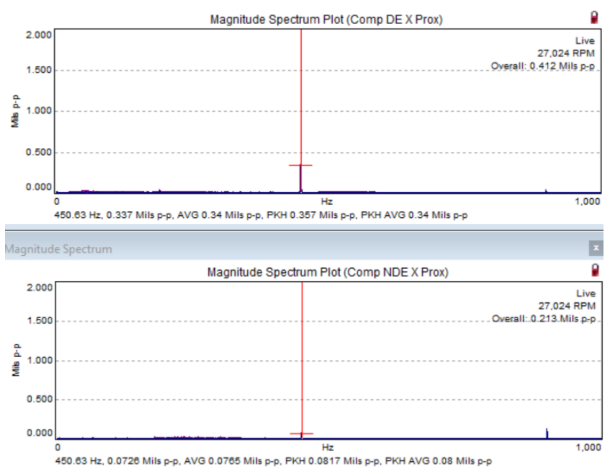

Figure 27 - Final Vibration Spectrum, -30 deg. IGV

Figure 28 plots the suction and discharge pressure during this final test. There are two internal pressure taps as shown in Figure 29. The plot shows a distinct difference between these two pressure taps (labeled as Diffuser-1 and Diffuser-2), especially as the compressor is throttled to near surge. The corresponding vibration orbits on the discharge end are also shown. The orbit becomes more elliptic due to radial forces caused by this non-uniform pressure, which is a normal consequence of a single-tongue volute collector. The bearings are able to accommodate this radial force, and no operational difficulties were encountered.

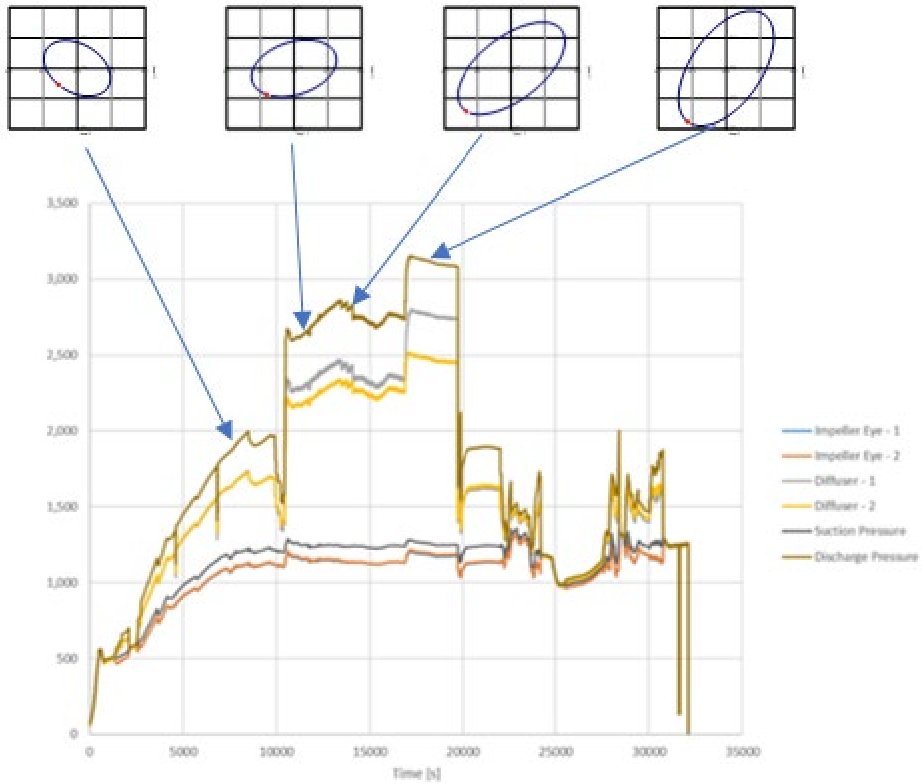

Figure 28 - Suction and Discharge Pressure (psia) vs. Time

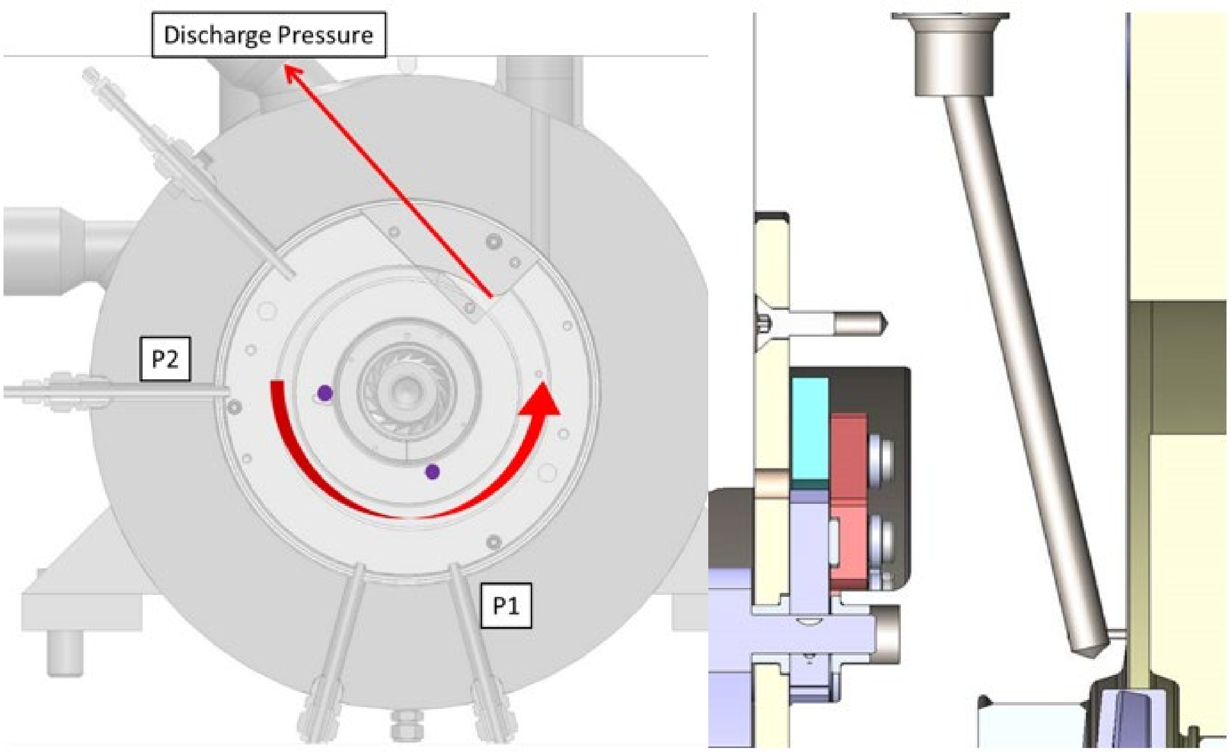

Figure 29 - Location of Internal Diffuser Pressure Taps

Bode plots (synchronous vibration vs. speed) were captured during the final shutdown of the compressor in Figure 30. The plots show smooth vibration behavior with a critical speed at around 12,600 rpm, which is reasonably close to the predicted first critical speed of 12,750 rpm previously presented in Figure 22. Overall, smooth behavior is observed during the coast down.

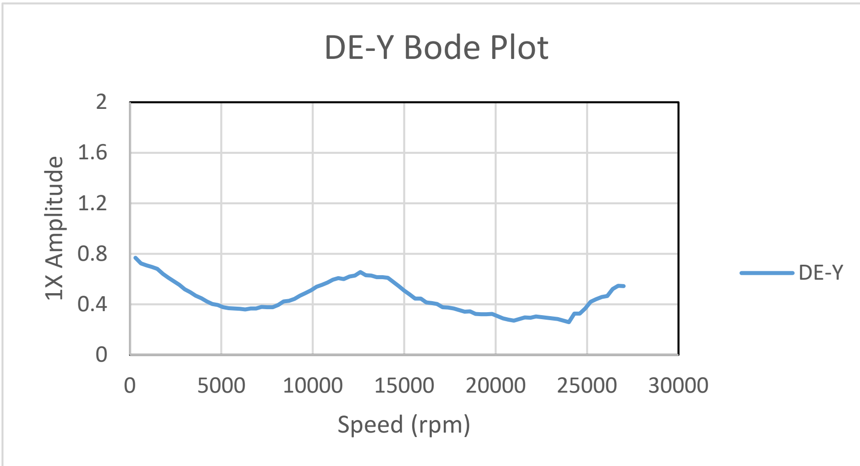

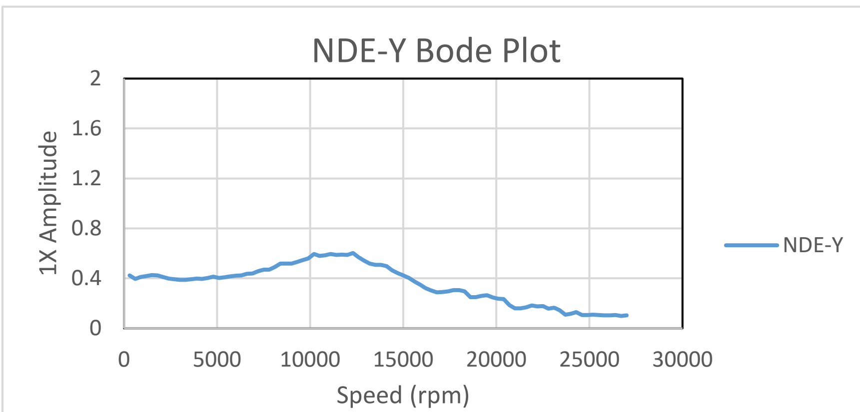

Figure 30 - Bode Plots During Final Rundown

PRESSURIZED COLD START

Pressure was maintained in the loop overnight following testing with 35ºC (95ºF) temperature and 83 bara (1,200 psia) suction pressure. The next morning, a cold start was initiated where the loop had cooled to 27ºC (80ºF) and the pressure reduced to 68.6 bara (995 psia), which is below the critical pressure, and the inlet conditions were multi-phase. The compressor was started to 5,000 rpm and then increased to 9,000 rpm with the cooling water turned off in an effort to warm the loop and thereby pressurizing it without having to add unnecessary mass that would later have to be blown off. The vibration levels and thrust position were both carefully monitored. Once 83 bara (1,200 psia) was achieved, the compressor was sped up.

Figure 31 shows the pressure-enthalpy (PH) diagram plotting the locus of points during the start and warming of the loop during the cold start. Once rotation occurred, multi-phase CO_2 was pulled from the loop and entered the compressor (light blue curve). As the loop heated up, the pressure increases and the supercritical regime were achieved. The dry gas seal supply gas was maintained well away from the liquid-vapor dome due to a seal gas supply heater.

The bearing vibration waterfall plot is shown in Figure 32 and shows some subsynchronous vibration, but the levels remained reasonably low. The thrust position was also monitored, and no abnormal behavior was observed. It should be noted that this test was performed before locking up the squeeze film dampers. The team does not see any issue in performing cold starts inside the liquid-vapor dome with CO_2 as long as the liquid is not allowed to enter the dry gas seals and the speed is kept low.

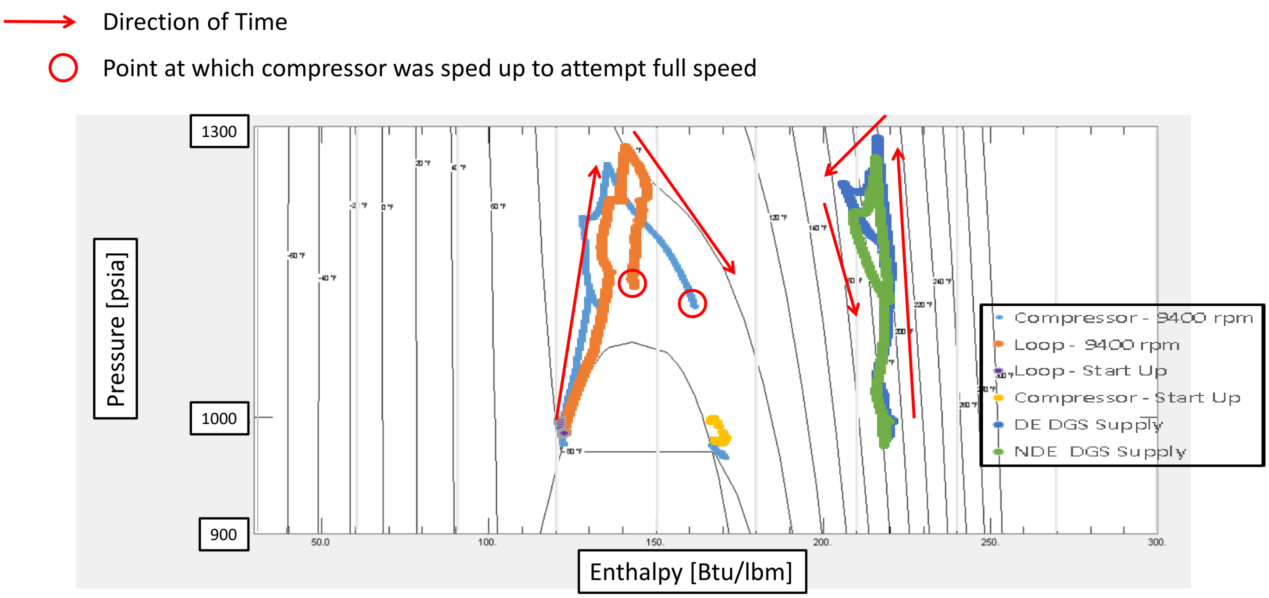

Figure 31 - Pressure-Enthalpy Diagram during Cold Start

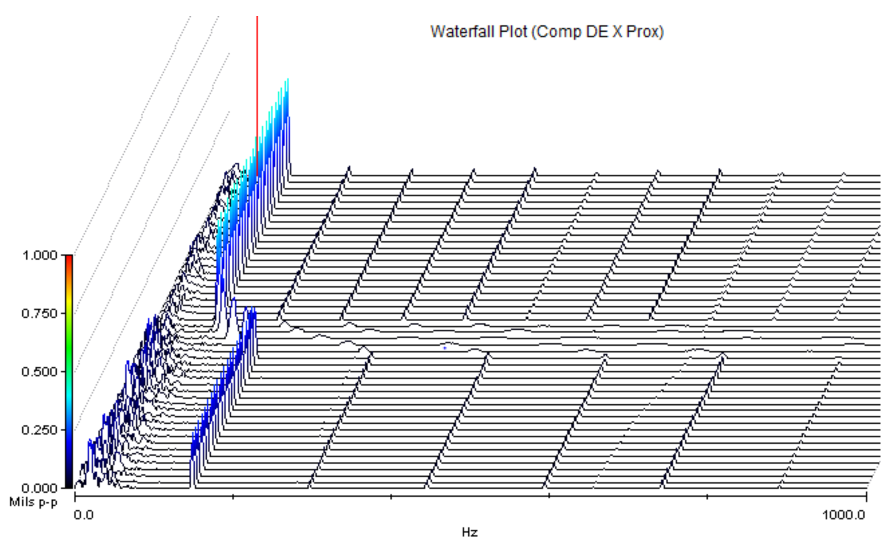

Figure 32 - Waterfall Plot of Radial Vibration during Cold Start

SUMMARY

The Apollo sCO_2 compressor development was able to achieve all of its mechanical objectives in terms of speed, pressure capability, stable rotordynamic behavior, and variable IGVs. Some challenges were encountered from a fluid induced subsynchronous vibration unlike traditional rotordynamic instabilities and rotating stall. The vibration amplitude was observed in test to be proportional to the inlet density. Many compressors operating in industry are likely to have unsteadiness due to separation off inlet guide vanes at certain operating conditions, but the high density of supercritical CO_2 acts to amplify these unsteady aerodynamic forces and is more pronounced in this class of compressor, especially if squeeze film dampers are utilized. By eliminating the SFDs, good vibration behavior was observed over a range of operating conditions and IGV setting angles and good agreement with predictions was demonstrated. A dry gas seal failure was encountered which was attributed to a material defect in the seal ring. A replacement seal from a different vendor ran successfully throughout the remaining test campaign. The volute forces acting on the rotor had an influence on the vibration orbits but were able to be accommodated by the bearings. The compressor executed a cold start inside the liquid-vapor dome without any operational issues. This accomplishment will permit future cold starts without the need to depressurize the loop at great operational savings and minimizing CO_2 release to the atmosphere.

REFERENCES

API, 2002, Axial and Centrifugal Compressors and Expander-Compressors for Petroleum, Chemical and Gas Industry Services, API Standard 617, Seventh Edition, American Petroleum Institute, Washington, D.C.

Cich, S., Moore, J., Mortzheim, J., and Hofer, D, 2018, “Design of a Supercritical CO_2 Compressor for use in a 10 MWe Power Cycle,” The 6th International Supercritical CO_2 Power Cycles Symposium, Pittsburgh, Pennsylvania, United States.

Cich, S., Moore, J., Towler, M., Mortzheim, J., and Hofer, D., 2019, “Loop Filling and Start Up with a Closed Loop sCO_2 Brayton Cycle,” ASME 2019 Turbo Expo, Phoenix, Arizona, United States.

Cich, S., Moore, J., Kulhanek, C., Mortzheim, J., 2020, “Development and Testing of a Supercritical CO_2 Compressor Operating Near the Dome, Turbomachinery and Pump Symposia, Texas A&M University, Houston, TX, September 15-17, 2020

Cich, S., Moore, J., Kulhanek, C., Towler, M., Mortzheim, J., 2021, “Mechanical Design and Testing of a 2.5 MW sCO_2 Compressor Loop,” Proceedings of the ASME Turbo Expo, GT2021-04155, June 7-11, 2021, Virtual Conference.

Ertas, B., Delgado, A., and Moore, J., 2018, “Dynamic Characterization of an Integral Squeeze Film Bearing Support Damper for a Supercritical CO_2 Expander,” Journal of Engineering for Gas Turbines and Power.

Hexemer, M, 2014, “Supercritical CO_2 Brayton Recompression Cycle Design and Control Features to Support Startup and Operation,” The 4th International Symposium – Supercritical CO_2 Power Cycles: Technologies for Transformational Energy Conversion, Pittsburgh, Pennsylvania, USA.

McClung, A., Smith, N., Allison, T., and Tom, B., 2018, “Practical Considerations for the Conceptual Design of an sCO2 Cycle,” 6th International Supercritical CO2 Power Cycles Symposium, Pittsburgh, Pennsylvania, United States.

Moore, J.J., Camatti, M., Smalley, A.J., Vannini, G.V., Vermin, L.L., 2006, Investigation of a

Rotordynamic Instability in a High Pressure Centrifugal Compressor Due to Damper Seal Clearance Divergence, 7th International Conference on Rotor Dynamics, September 25-28, 2006, Vienna, Austria.

Moore, J. J., Ransom, D. L., and Viana, F., 2007, “Rotordynamic Force Prediction of Centrifugal Compressor Impellers Using Computational Fluid Dynamics,” ASME Paper No. GT2007-28181.

Moore, J.J., Evans, N., Brun, K., Kalra, C., 2015, “Development of 1 MWe Supercritical CO_2 Test Loop,” Proceedings of the ASME Turbo Expo, Paper #GT2015-43771, June 15-19, 2015, Montreal, Quebec, Canada.

Moore, J.J., Cich, S., Day-Towler, M., Hofer, D., Mortzheim, J., 2018, “Testing of a 10 MWe Supercritical CO2 Turbine,” Proceedings of 47th Turbomachinery Symposium, Houston, TX, September 2018.

Moore, J.J., Cich, S., Day-Towler, M., Mortzheim, J., 2020, “Development and Testing of a 10 MWe Supercritical CO2 Turbine in a 1 MWe Flow Loop,” GT2020-13894, Proceedings of the ASME 2020 Turbo Expo Turbomachinery Technical Conference & Exposition, June 22-26, 2020, London, England

Sezal, I., Chen, N., Aalburg, C., Gadamsetty, R., Erhard, W., Del Greco, A., Tapinassi, L., and Lang, M., 2016, “Introduction of Circumferentially Non-uniform Variable Guide Vanes in the Inlet Plenum of a Centrifugal Compressor for Minimum Losses and Flow Distortion,” Journal of Turbomachinery, September 2016, Vol. 138.

Spadacini, C., Pesatori, E., Centemeri, Lazzarin, N., Macchi, R., and Sanvito, M., 2018, “Optimized Cycle and Turbomachinery Configuration for an Intercooled, Recompressed sCO_2 Cycle,” The 6th International Supercritical CO_2 Power Cycles. Symposium, Pittsburgh, Pennsylvania, United States

ACKNOWLEDGEMENTS

The authors want to thank the U.S. Department of Energy, Office of Energy Efficiency and Renewable Energy (EERE), which funded this work under Award Number DE-EE0007109. Thanks also to Ellen Smith of SwRI for performing the CFD analysis on the inlet and to Chris Kulhanek and Justin Hollingsworth for their rotordynamic predictions.

DISCLAIMER